

Search for hidden-charm tetraquark with strangeness in

$$e^+e^- \rightarrow K^+ D_s^{*-} D^{*0} + c.c. \quad *$$

M. Ablikim(麦迪娜)¹, M. N. Achasov^{12,b}, P. Adlarson⁷², M. Albrecht⁴, R. Aliberti³³, A. Amoroso^{71A,71C}, M. R. An(安美儒)³⁷, Q. An(安琪)^{68,55}, Y. Bai(白羽)⁵⁴, O. Bakina³⁴, R. Baldini Ferroli^{27A}, I. Balossino^{28A}, Y. Ban(班勇)^{44,g}, V. Batozskaya^{1,42}, D. Becker³³, K. Begzsuren³⁰, N. Berger³³, M. Bertani^{27A}, D. Bettoni^{28A}, F. Bianchi^{71A,71C}, E. Bianco^{71A,71C}, J. Bloms⁶⁵, A. Bortone^{71A,71C}, I. Boyko³⁴, R. A. Briere⁵, A. Brueggemann⁶⁵, H. Cai(蔡浩)⁷³, X. Cai(蔡啸)^{1,55}, A. Calcaterra^{27A}, G. F. Cao(曹国富)^{1,60}, N. Cao(曹宁)^{1,60}, S. A. Cetin^{59A}, J. F. Chang(常劲帆)^{1,55}, W. L. Chang(常万玲)^{1,60}, G. R. Che(车国荣)⁴¹, G. Chelkov^{34,a}, C. Chen(陈琛)⁴¹, Chao Chen(陈超)⁵², G. Chen(陈刚)¹, H. S. Chen(陈和生)^{1,60}, M. L. Chen(陈玛丽)^{1,55,60}, S. J. Chen(陈申见)⁴⁰, S. M. Chen(陈少敏)⁵⁸, T. Chen^{1,60}, X. R. Chen(陈旭荣)^{29,60}, X. T. Chen^{1,60}, Y. B. Chen(陈元柏)^{1,55}, Z. J. Chen(陈卓俊)^{24,h}, W. S. Cheng(成伟帅)^{71C}, S. K. Choi⁵², X. Chu(初晓)⁴¹, G. Cibinetto^{28A}, F. Cossio^{71C}, J. J. Cui(崔佳佳)⁴⁷, H. L. Dai(代洪亮)^{1,55}, J. P. Dai(代建平)⁷⁶, A. Dbeyssi¹⁸, R. E. de Boer⁴, D. Dedovich³⁴, Z. Y. Deng(邓子艳)¹, A. Denig³³, I. Denysenko³⁴, M. Destefanis^{71A,71C}, F. De Mori^{71A,71C}, Y. Ding(丁勇)³⁸, Y. Ding(丁逸)³², J. Dong(董静)^{1,55}, L. Y. Dong(董燎原)^{1,60}, M. Y. Dong(董明义)^{1,55,60}, X. Dong(董翔)⁷³, S. X. Du(杜书先)⁷⁸, Z. H. Duan(段宗欢)⁴⁰, P. Egorov^{34,a}, Y. L. Fan(范玉兰)⁷³, J. Fang(方建)^{1,55}, S. S. Fang(房双世)^{1,60}, W. X. Fang(方文兴)¹, Y. Fang(方易)¹, R. Farinelli^{28A}, L. Fava^{71B,71C}, F. Feldbauer⁴, G. Felici^{27A}, C. Q. Feng(封常青)^{68,55}, J. H. Feng(冯俊华)⁵⁶, K. Fischer⁶⁶, M. Fritsch⁴, C. Fritzsche⁶⁵, C. D. Fu(傅成栋)¹, H. Gao(高涵)⁶⁰, Y. N. Gao(高原宁)^{44,g}, Yang Gao(高扬)^{68,55}, S. Garbolino^{71C}, I. Garzia^{28A,28B}, P. T. Ge(葛潘婷)⁷³, Z. W. Ge(葛振武)⁴⁰, C. Geng(耿聪)⁵⁶, E. M. Gersabeck⁶⁴, A. Gilman⁶⁶, K. Goetzen¹³, L. Gong(龚丽)³⁸, W. X. Gong(龚文煊)^{1,55}, W. Gradl³³, M. Greco^{71A,71C}, L. M. Gu(谷立民)⁴⁰, M. H. Gu(顾皓)^{1,55}, Y. T. Gu(顾运斤)¹⁵, C. Y. Guan(关春懿)^{1,60}, A. Q. Guo(郭爱强)^{29,60}, L. B. Guo(郭立波)³⁹, R. P. Guo(郭如盼)⁴⁶, Y. P. Guo(郭玉萍)^{11,f}, A. Guskov^{34,a}, W. Y. Han(韩文颖)³⁷, X. Q. Hao(郝喜庆)¹⁹, F. A. Harris⁶², K. K. He(何凯凯)⁵², K. L. He(何康林)^{1,60}, F. H. Heinsius⁴, C. H. Heinz³³, Y. K. Heng(衡月昆)^{1,55,60}, C. Herold⁵⁷, G. Y. Hou(侯国一)^{1,60}, Y. R. Hou(侯颖锐)⁶⁰, Z. L. Hou(侯治龙)¹, H. M. Hu(胡海明)^{1,60}, J. F. Hu^{53,i}, T. Hu(胡涛)^{1,55,60}, Y. Hu(胡誉)¹, G. S. Huang(黄光顺)^{68,55}, K. X. Huang(黄凯旋)⁵⁶, L. Q. Huang(黄麟钦)^{29,60}, X. T. Huang(黄性涛)⁴⁷, Y. P. Huang(黄燕萍)¹, Z. Huang(黄震)^{44,g}, T. Hussain⁷⁰, N. Hüskens^{26,33}, W. Imoehl²⁶, M. Irshad^{68,55}, J. Jackson²⁶, S. Jaeger⁴, S. Janchiv³⁰, E. Jang⁵², J. H. Jeong⁵², Q. Ji(纪全)¹, Q. P. Ji(姬清平)¹⁹, X. B. Ji(季晓斌)^{1,60}, X. L. Ji(季筱璐)^{1,55}, Y. Y. Ji(吉钰瑶)⁴⁷, Z. K. Jia(贾泽坤)^{68,55}, P. C. Jiang(蒋沛成)^{44,g}, S. S. Jiang(姜赛赛)³⁷, X. S. Jiang(江晓山)^{1,55,60}, Y. Jiang⁶⁰, J. B. Jiao(焦健斌)⁴⁷, Z. Jiao(焦铮)²², S. Jin(金山)⁴⁰, Y. Jin(金毅)⁶³, M. Q. Jing(荆茂强)^{1,60}, T. Johansson⁷², S. Kabana³¹, N. Kalantar-Nayestanaki⁶¹, X. L. Kang(康晓琳)⁹, X. S. Kang(康晓琳)³⁸, R. Kappert⁶¹, M. Kavatsyuk⁶¹, B. C. Ke(柯百谦)⁷⁸, I. K. Keshk⁴, A. Khoukaz⁶⁵, R. Kiuchi¹, R. Kliemt¹³, L. Koch³⁵, O. B. Kolcu^{59A}, B. Kopf⁴, M. Kuemmel⁴, M. Kuessner⁴, A. Kupsc^{42,72}, W. Kühn³⁵, J. J. Lane⁶⁴, J. S. Lange³⁵, P. Larin¹⁸, A. Lavania²⁵, L. Lavezzi^{71A,71C}, T. T. Lei(雷天天)^{68,k}, Z. H. Lei(雷祚弘)^{68,55}, H. Leithoff³³, M. Lellmann³³, T. Lenz³³, C. Li(李聪)⁴¹, C. Li(李翠)⁴⁵, C. H. Li(李春花)³⁷,

Received xxxx June xxxx

* Supported in part by National Key R&D Program of China under Contracts Nos. 2020YFA0406400, 2020YFA0406300; National Natural Science Foundation of China (NSFC) under Contracts Nos. 11635010, 11735014, 11805086, 11835012, 11935015, 11935016, 11935018, 11961141012, 12022510, 12025502, 12035009, 12035013, 12192260, 12192261, 12192262, 12192263, 12192264, 12192265; the Chinese Academy of Sciences (CAS) Large-Scale Scientific Facility Program; Joint Large-Scale Scientific Facility Funds of the NSFC and CAS under Contract No. U1832207; the CAS Center for Excellence in Particle Physics (CCEPP); 100 Talents Program of CAS; Fundamental Research Funds for the Central Universities, Lanzhou University, University of Chinese Academy of Sciences; The Institute of Nuclear and Particle Physics (INPAC) and Shanghai Key Laboratory for Particle Physics and Cosmology; ERC under Contract No. 758462; European Union's Horizon 2020 research and innovation programme under Marie Skłodowska-Curie grant agreement under Contract No. 894790; German Research Foundation DFG under Contracts Nos. 443159800, Collaborative Research Center CRC 1044, GRK 2149; Istituto Nazionale di Fisica Nucleare, Italy; Ministry of Development of Turkey under Contract No. DPT2006K-120470; National Science and Technology fund; National Science Research and Innovation Fund (NSRF) via the Program Management Unit for Human Resources & Institutional Development, Research and Innovation under Contract No. B16F640076; Olle Engkvist Foundation under Contract No. 200-0605; STFC (United Kingdom); Suranaree University of Technology (SUT), Thailand Science Research and Innovation (TSRI), and National Science Research and Innovation Fund (NSRF) under Contract No. 160355; The Royal Society, UK under Contracts Nos. DH140054, DH160214; The Swedish Research Council; U. S. Department of Energy under Contract No. DE-FG02-05ER41374.

Cheng Li(李澄)^{68,55}, D. M. Li(李德民)⁷⁸, F. Li(李飞)^{1,55}, G. Li(李刚)¹, H. Li(李慧)⁴⁹, H. Li(李贺)^{68,55}, H. B. Li(李海波)^{1,60}, H. J. Li(李惠静)¹⁹, H. N. Li^{53,i}, J. Q. Li⁴, J. S. Li(李静舒)⁵⁶, J. W. Li(李井文)⁴⁷, Ke Li(李科)¹, L. J. Li^{1,60}, L. K. Li(李龙科)¹, Lei Li(李蕾)³, M. H. Li(李明浩)⁴¹, P. R. Li(李培荣)^{36,j,k}, S. X. Li(李素娴)¹¹, S. Y. Li(栗帅迎)⁵⁸, T. Li(李腾)⁴⁷, W. D. Li(李卫东)^{1,60}, W. G. Li(李卫国)¹, X. H. Li(李旭红)^{68,55}, X. L. Li(李晓玲)⁴⁷, Xiaoyu Li(李晓宇)^{1,60}, Y. G. Li(李彦谷)^{44,g}, Z. X. Li(李振轩)¹⁵, Z. Y. Li(李紫源)⁵⁶, C. Liang(梁畅)⁴⁰, H. Liang(梁浩)^{1,60}, H. Liang(梁浩)³², H. Liang(梁昊)^{68,55}, Y. F. Liang(梁勇飞)⁵¹, Y. T. Liang(梁羽铁)^{29,60}, G. R. Liao(廖广睿)¹⁴, L. Z. Liao(廖龙洲)⁴⁷, J. Libby²⁵, A. Limphirat⁵⁷, C. X. Lin(林创新)⁵⁶, D. X. Lin(林德旭)^{29,60}, T. Lin¹, B. J. Liu(刘北江)¹, C. Liu(刘成)³², C. X. Liu(刘春秀)¹, D. Liu^{18,68}, F. H. Liu(刘福虎)⁵⁰, Fang Liu(刘芳)¹, Feng Liu(刘峰)⁶, G. M. Liu^{53,i}, H. Liu^{36,j,k}, H. B. Liu(刘宏邦)¹⁵, H. M. Liu(刘怀民)^{1,60}, Huanhuan Liu(刘欢欢)¹, Huihui Liu(刘汇慧)²⁰, J. B. Liu(刘建北)^{68,55}, J. L. Liu(刘佳俊)⁶⁹, J. Y. Liu(刘晶译)^{1,60}, K. Liu(刘凯)¹, K. Y. Liu(刘魁勇)³⁸, Ke Liu(刘珂)²¹, L. Liu(刘亮)^{68,55}, Lu Liu(刘露)⁴¹, M. H. Liu(刘美宏)^{11,f}, P. L. Liu(刘佩莲)¹, Q. Liu(刘倩)⁶⁰, S. B. Liu(刘树彬)^{68,55}, T. Liu(刘桐)^{11,f}, W. K. Liu(刘维克)⁴¹, W. M. Liu(刘卫民)^{68,55}, X. Liu(刘翔)^{36,j,k}, Y. Liu(刘英)^{36,j,k}, Y. B. Liu(刘玉斌)⁴¹, Z. A. Liu(刘振安)^{1,55,60}, Z. Q. Liu(刘智青)⁴⁷, X. C. Lou(娄辛丑)^{1,55,60}, F. X. Lu(卢飞翔)⁵⁶, H. J. Lu(吕海江)²², J. G. Lu(吕军光)^{1,55}, X. L. Lu(陆小玲)¹, Y. Lu(卢宇)⁷, Y. P. Lu(卢云鹏)^{1,55}, Z. H. Lu(卢泽辉)^{1,60}, C. L. Luo(罗成林)³⁹, M. X. Luo(罗民兴)⁷⁷, T. Luo(罗涛)^{11,f}, X. L. Luo(罗小兰)^{1,55}, X. R. Lyu(吕晓睿)⁶⁰, Y. F. Lyu(吕翌丰)⁴¹, F. C. Ma(马风才)³⁸, H. L. Ma(马海龙)¹, L. L. Ma(马连良)⁴⁷, M. M. Ma(马明明)^{1,60}, Q. M. Ma(马秋梅)¹, R. Q. Ma(马润秋)^{1,60}, R. T. Ma(马瑞廷)⁶⁰, X. Y. Ma(马晓妍)^{1,55}, Y. Ma(马尧)^{44,g}, F. E. Maas¹⁸, M. Maggiora^{71A,71C}, S. Maldaner⁴, S. Malde⁶⁶, Q. A. Malik⁷⁰, A. Mangoni^{27B}, Y. J. Mao(冒亚军)^{44,g}, Z. P. Mao(毛泽普)¹, S. Marcello^{71A,71C}, Z. X. Meng(孟召霞)⁶³, J. G. Messchendorp^{13,61}, G. Mezzadri^{28A}, H. Miao^{1,60}, T. J. Min(闵天觉)⁴⁰, R. E. Mitchell²⁶, X. H. Mo(莫晓虎)^{1,55,60}, N. Yu. Muchnoi^{12,b}, Y. Nefedov³⁴, F. Nerling^{18,d}, I. B. Nikolaev^{12,b}, Z. Ning(宁哲)^{1,55}, S. Nisar^{10,i}, Y. Niu(牛艳)⁴⁷, S. L. Olsen⁶⁰, Q. Ouyang(欧阳群)^{1,55,60}, S. Pacetti^{27B,27C}, X. Pan(潘祥)^{11,f}, Y. Pan(潘越)⁵⁴, A. Pathak³², Y. P. Pei(裴宇鹏)^{68,55}, M. Pelizaes⁴, H. P. Peng(彭海平)^{68,55}, K. Peters^{13,d}, J. L. Ping(平加伦)³⁹, R. G. Ping(平荣刚)^{1,60}, S. Plura³³, S. Pogodin³⁴, V. Prasad^{68,55}, F. Z. Qi(齐法制)¹, H. Qi(齐航)^{68,55}, H. R. Qi(漆红荣)⁵⁸, M. Qi(祁鸣)⁴⁰, T. Y. Qi(齐天钰)^{11,f}, S. Qian(钱森)^{1,55}, W. B. Qian(钱文斌)⁶⁰, Z. Qian(钱钊)⁵⁶, C. F. Qiao(乔从丰)⁶⁰, J. J. Qin(秦佳佳)⁶⁹, L. Q. Qin(秦丽清)¹⁴, X. P. Qin(覃潇平)^{11,f}, X. S. Qin(秦小帅)⁴⁷, Z. H. Qin(秦中华)^{1,55}, J. F. Qiu(邱进发)¹, S. Q. Qu(屈三强)⁵⁸, K. H. Rashid⁷⁰, C. F. Redmer³³, K. J. Ren(任旷洁)³⁷, A. Rivetti^{71C}, V. Rodin⁶¹, M. Rolo^{71C}, G. Rong(荣刚)^{1,60}, Ch. Rosner¹⁸, S. N. Ruan(阮氏宁)⁴¹, A. Sarantsev^{34,c}, Y. Schelhaas³³, C. Schnier⁴, K. Schoenning⁷², M. Scodeggio^{28A,28B}, K. Y. Shan(尚科羽)^{11,f}, W. Shan(单威)²³, X. Y. Shan(单心钰)^{68,55}, J. F. Shangguan(上官剑锋)⁵², L. G. Shao(邵立港)^{1,60}, M. Shao(邵明)^{68,55}, C. P. Shen(沈成平)^{11,f}, H. F. Shen(沈宏飞)^{1,60}, W. H. Shen(沈文涵)⁶⁰, X. Y. Shen(沈肖雁)^{1,60}, B. A. Shi(施伯安)⁶⁰, H. C. Shi(石煌超)^{68,55}, J. Y. Shi(石京燕)¹, q. q. Shi(石勤强)⁵², R. S. Shi(师荣盛)^{1,60}, X. Shi(史欣)^{1,55}, J. J. Song(宋娇娇)¹⁹, W. M. Song(宋维民)^{32,1}, Y. X. Song(宋响轩)^{44,g}, S. Sosio^{71A,71C}, S. Spataro^{71A,71C}, F. Stieler³³, P. P. Su(苏彭彭)⁵², Y. J. Su(粟杨捷)⁶⁰, G. X. Sun(孙功星)¹, H. Sun⁶⁰, H. K. Sun(孙浩凯)¹, J. F. Sun(孙俊峰)¹⁹, L. Sun(孙亮)⁷³, S. S. Sun(孙胜森)^{1,60}, T. Sun(孙童)^{1,60}, W. Y. Sun(孙文玉)³², Y. J. Sun(孙勇杰)^{68,55}, Y. Z. Sun(孙永昭)¹, Z. T. Sun(孙振田)⁴⁷, Y. H. Tan(谭英华)⁷³, Y. X. Tan(谭雅星)^{68,55}, C. J. Tang(唐昌建)⁵¹, G. Y. Tang(唐光毅)¹, J. Tang(唐健)⁵⁶, L. Y. Tao(陶璐燕)⁶⁹, Q. T. Tao(陶秋田)^{24,h}, M. Tat⁶⁶, J. X. Teng(滕佳秀)^{68,55}, V. Thoren⁷², W. H. Tian(田文辉)⁴⁹, Y. Tian(田野)^{29,60}, I. Uman^{59B}, B. Wang(王斌)¹, B. Wang(王博)^{68,55}, B. L. Wang(王滨龙)⁶⁰, C. W. Wang(王成伟)⁴⁰, D. Y. Wang(王大勇)^{44,g}, F. Wang(王菲)⁶⁹, H. J. Wang(王泓鉴)^{36,j,k}, H. P. Wang(王宏鹏)^{1,60}, K. Wang(王科)^{1,55}, L. L. Wang(王亮亮)¹, M. Wang(王萌)⁴⁷, M. Z. Wang(王梦真)^{44,g}, Meng Wang(王蒙)^{1,60}, S. Wang(王顺)^{11,f}, S. Wang¹⁴, T. Wang(王婷)^{11,f}, T. J. Wang(王腾蛟)⁴¹, W. Wang(王为)⁵⁶, W. H. Wang(王文欢)⁷³, W. P. Wang(王维平)^{68,55}, X. Wang(王轩)^{44,g}, X. F. Wang(王雄飞)^{36,j,k}, X. L. Wang(王小龙)^{11,f}, Y. Wang(王亦)⁵⁸, Y. D. Wang(王雅迪)⁴³, Y. F. Wang(王贻芳)^{1,55,60}, Y. H. Wang(王英豪)⁴⁵, Y. Q. Wang(王雨晴)¹, Yaqian Wang(王亚乾)^{17,1}, Z. Wang(王铮)^{1,55}, Z. Y. Wang(王至勇)^{1,60}, Ziyi Wang(王子一)⁶⁰, D. H. Wei(魏代会)¹⁴, F. Weidner⁶⁵, S. P. Wen(文硕频)¹, D. J. White⁶⁴, U. Wiedner⁴, G. Wilkinson⁶⁶, M. Wolke⁷², L. Wollenberg⁴, J. F. Wu(吴金飞)^{1,60}, L. H. Wu(伍灵慧)¹, L. J. Wu(吴连近)^{1,60}, X. Wu(吴潇)^{11,f}, X. H. Wu(伍雄浩)³², Y. Wu⁶⁸, Y. J. Wu(吴英杰)²⁹, Z. Wu(吴智)^{1,55}, L. Xia(夏磊)^{68,55}, T. Xiang(相腾)^{44,g}, D. Xiao(肖栋)^{36,j,k}, G. Y. Xiao(肖光延)⁴⁰, H. Xiao(肖浩)^{11,f}, S. Y. Xiao(肖素玉)¹, Y. L. Xiao(肖云龙)^{11,f}, Z. J. Xiao(肖振军)³⁹, C. Xie(谢陈)⁴⁰, X. H. Xie(谢昕华)^{44,g}, Y. Xie(谢勇)⁴⁷, Y. G. Xie(谢宇广)^{1,55}, Y. H. Xie(谢跃红)⁶, Z. P. Xie(谢智鹏)^{68,55}, T. Y. Xing(邢天宇)^{1,60}, C. F. Xu^{1,60}, C. J. Xu(许创杰)⁵⁶, G. F. Xu(许国发)¹, H. Y. Xu(许皓月)⁶³, Q. J. Xu(徐庆君)¹⁶, X. P. Xu(徐新平)⁵², Y. C. Xu(胥英超)⁷⁵, Z. P. Xu(许泽鹏)⁴⁰, F. Yan(严芳)^{11,f}, L. Yan(严亮)^{11,f}, W. B. Yan(鄢文标)^{68,55}, W. C. Yan(闫文成)⁷⁸, H. J. Yang(杨海军)^{48,e}, H. L. Yang(杨昊霖)³², H. X. Yang(杨洪勋)¹, Tao Yang(杨涛)¹, Y. F. Yang(杨艳芳)⁴¹, Y. X. Yang(杨逸翔)^{1,60}, Yifan Yang(杨翊凡)^{1,60}, M. Ye(叶梅)^{1,55}, M. H. Ye(叶铭汉)⁸, J. H. Yin(殷俊昊)¹, Z. Y. You(尤郑昀)⁵⁶, B. X. Yu(俞伯祥)^{1,55,60}, C. X. Yu(喻绝旭)⁴¹, G. Yu(余刚)^{1,60}, T. Yu(于涛)⁶⁹, X. D. Yu(余旭东)^{44,g}, C. Z. Yuan(苑长征)^{1,60}, L. Yuan(袁丽)², S. C. Yuan¹, X. Q. Yuan(袁晓庆)¹, Y. Yuan(袁野)^{1,60}, Z. Y. Yuan(袁朝阳)⁵⁶, C. X. Yue(岳崇兴)³⁷, A. A. Zafar⁷⁰, F. R. Zeng(曾凡蕊)⁴⁷, X. Zeng(曾鑫)⁶, Y. Zeng(曾云)^{24,h}, X. Y. Zhai(翟星晔)³², Y. H. Zhan(詹永华)⁵⁶, A. Q. Zhang(张安庆)^{1,60}, B. L. Zhang^{1,60}, B. X. Zhang(张丙新)¹, D. H. Zhang(张丹昊)⁴¹, G. Y. Zhang(张广义)¹⁹, H. Zhang⁶⁸, H. H. Zhang(张宏宏)³², H. H. Zhang(张宏浩)⁵⁶, H. Q. Zhang(张华桥)^{1,55,60}, H. Y. Zhang(章红宇)^{1,55}, J. L. Zhang(张杰磊)⁷⁴, J. Q. Zhang(张敬

庆)³⁹, J. W. Zhang(张家文)^{1,55,60}, J. X. Zhang^{36,j,k}, J. Y. Zhang(张建勇)¹, J. Z. Zhang(张景芝)^{1,60}, Jianyu Zhang(张剑宇)^{1,60}, Jiawei Zhang(张嘉伟)^{1,60}, L. M. Zhang(张黎明)⁵⁸, L. Q. Zhang(张丽青)⁵⁶, Lei Zhang(张雷)⁴⁰, P. Zhang¹, Q. Y. Zhang(张秋岩)^{37,78}, Shuihan Zhang(张水涵)^{1,60}, Shulei Zhang(张书磊)^{24,h}, X. D. Zhang(张小东)⁴³, X. M. Zhang¹, X. Y. Zhang(张学尧)⁴⁷, X. Y. Zhang(张旭颜)⁵², Y. Zhang⁶⁶, Y. T. Zhang(张亚腾)⁷⁸, Y. H. Zhang(张银鸿)^{1,55}, Yan Zhang(张言)^{68,55}, Yao Zhang(张瑶)¹, Z. H. Zhang¹, Z. L. Zhang(张兆领)³², Z. Y. Zhang(张子羽)⁴¹, Z. Y. Zhang(张振宇)⁷³, G. Zhao(赵光)¹, J. Zhao(赵静)³⁷, J. Y. Zhao(赵静宜)^{1,60}, J. Z. Zhao(赵京周)^{1,55}, Lei Zhao(赵雷)^{68,55}, Ling Zhao(赵玲)¹, M. G. Zhao(赵明刚)⁴¹, S. J. Zhao(赵书俊)⁷⁸, Y. B. Zhao(赵豫斌)^{1,55}, Y. X. Zhao(赵宇翔)^{29,60}, Z. G. Zhao(赵政国)^{68,55}, A. Zhemchugov^{34,a}, B. Zheng(郑波)⁶⁹, J. P. Zheng(郑建平)^{1,55}, Y. H. Zheng(郑阳恒)⁶⁰, B. Zhong(钟彬)³⁹, C. Zhong(钟翠)⁶⁹, X. Zhong(钟鑫)⁵⁶, H. Zhou(周航)⁴⁷, L. P. Zhou(周利鹏)^{1,60}, X. Zhou(周详)⁷³, X. K. Zhou(周晓康)⁶⁰, X. R. Zhou(周小蓉)^{68,55}, X. Y. Zhou(周兴玉)³⁷, Y. Z. Zhou(周卓)^{11,f}, J. Zhu(朱江)⁴¹, K. Zhu(朱凯)¹, K. J. Zhu(朱科军)^{1,55,60}, L. X. Zhu(朱琳莹)⁶⁰, S. H. Zhu(朱世海)⁶⁷, S. Q. Zhu(朱仕强)⁴⁰, T. J. Zhu(朱腾蛟)⁷⁴, W. J. Zhu(朱文静)^{11,f}, Y. C. Zhu(朱莹春)^{68,55}, Z. A. Zhu(朱自安)^{1,60}, J. H. Zou(邹佳恒)¹, J. Zu(祖健)^{68,55}

(BESIII Collaboration)

¹ Institute of High Energy Physics, Beijing 100049, People's Republic of China

² Beihang University, Beijing 100191, People's Republic of China

³ Beijing Institute of Petrochemical Technology, Beijing 102617, People's Republic of China

⁴ Bochum Ruhr-University, D-44780 Bochum, Germany

⁵ Carnegie Mellon University, Pittsburgh, Pennsylvania 15213, USA

⁶ Central China Normal University, Wuhan 430079, People's Republic of China

⁷ Central South University, Changsha 410083, People's Republic of China

⁸ China Center of Advanced Science and Technology, Beijing 100190, People's Republic of China

⁹ China University of Geosciences, Wuhan 430074, People's Republic of China

¹⁰ COMSATS University Islamabad, Lahore Campus, Defence Road, Off Raiwind Road, 54000 Lahore, Pakistan

¹¹ Fudan University, Shanghai 200433, People's Republic of China

¹² G.I. Budker Institute of Nuclear Physics SB RAS (BINP), Novosibirsk 630090, Russia

¹³ GSI Helmholtzcentre for Heavy Ion Research GmbH, D-64291 Darmstadt, Germany

¹⁴ Guangxi Normal University, Guilin 541004, People's Republic of China

¹⁵ Guangxi University, Nanning 530004, People's Republic of China

¹⁶ Hangzhou Normal University, Hangzhou 310036, People's Republic of China

¹⁷ Hebei University, Baoding 071002, People's Republic of China

¹⁸ Helmholtz Institute Mainz, Staudinger Weg 18, D-55099 Mainz, Germany

¹⁹ Henan Normal University, Xinxiang 453007, People's Republic of China

²⁰ Henan University of Science and Technology, Luoyang 471003, People's Republic of China

²¹ Henan University of Technology, Zhengzhou 450001, People's Republic of China

²² Huangshan College, Huangshan 245000, People's Republic of China

²³ Hunan Normal University, Changsha 410081, People's Republic of China

²⁴ Hunan University, Changsha 410082, People's Republic of China

²⁵ Indian Institute of Technology Madras, Chennai 600036, India

²⁶ Indiana University, Bloomington, Indiana 47405, USA

²⁷ INFN Laboratori Nazionali di Frascati, (A)INFN Laboratori Nazionali di Frascati, I-00044, Frascati, Italy;

(B)INFN Sezione di Perugia, I-06100, Perugia, Italy; (C)University of Perugia, I-06100, Perugia, Italy

²⁸ INFN Sezione di Ferrara, (A)INFN Sezione di Ferrara, I-44122, Ferrara, Italy; (B)University of Ferrara, I-44122, Ferrara, Italy

²⁹ Institute of Modern Physics, Lanzhou 730000, People's Republic of China

³⁰ Institute of Physics and Technology, Peace Avenue 54B, Ulaanbaatar 13330, Mongolia

³¹ Instituto de Alta Investigación, Universidad de Tarapacá, Casilla 7D, Arica, Chile

³² Jilin University, Changchun 130012, People's Republic of China

³³ Johannes Gutenberg University of Mainz, Johann-Joachim-Becher-Weg 45, D-55099 Mainz, Germany

³⁴ Joint Institute for Nuclear Research, 141980 Dubna, Moscow region, Russia

³⁵ Justus-Liebig-Universität Giessen, II. Physikalisches Institut, Heinrich-Buff-Ring 16, D-35392 Giessen, Germany

³⁶ Lanzhou University, Lanzhou 730000, People's Republic of China

³⁷ Liaoning Normal University, Dalian 116029, People's Republic of China

³⁸ Liaoning University, Shenyang 110036, People's Republic of China

³⁹ Nanjing Normal University, Nanjing 210023, People's Republic of China

⁴⁰ Nanjing University, Nanjing 210093, People's Republic of China

⁴¹ Nankai University, Tianjin 300071, People's Republic of China

- ⁴² National Centre for Nuclear Research, Warsaw 02-093, Poland
- ⁴³ North China Electric Power University, Beijing 102206, People's Republic of China
- ⁴⁴ Peking University, Beijing 100871, People's Republic of China
- ⁴⁵ Qufu Normal University, Qufu 273165, People's Republic of China
- ⁴⁶ Shandong Normal University, Jinan 250014, People's Republic of China
- ⁴⁷ Shandong University, Jinan 250100, People's Republic of China
- ⁴⁸ Shanghai Jiao Tong University, Shanghai 200240, People's Republic of China
- ⁴⁹ Shanxi Normal University, Linfen 041004, People's Republic of China
- ⁵⁰ Shanxi University, Taiyuan 030006, People's Republic of China
- ⁵¹ Sichuan University, Chengdu 610064, People's Republic of China
- ⁵² Soochow University, Suzhou 215006, People's Republic of China
- ⁵³ South China Normal University, Guangzhou 510006, People's Republic of China
- ⁵⁴ Southeast University, Nanjing 211100, People's Republic of China
- ⁵⁵ State Key Laboratory of Particle Detection and Electronics, Beijing 100049, Hefei 230026, People's Republic of China
- ⁵⁶ Sun Yat-Sen University, Guangzhou 510275, People's Republic of China
- ⁵⁷ Suranaree University of Technology, University Avenue 111, Nakhon Ratchasima 30000, Thailand
- ⁵⁸ Tsinghua University, Beijing 100084, People's Republic of China
- ⁵⁹ Turkish Accelerator Center Particle Factory Group, (A)Istinye University, 34010, Istanbul, Turkey; (B)Near East University, Nicosia, North Cyprus, Mersin 10, Turkey
- ⁶⁰ University of Chinese Academy of Sciences, Beijing 100049, People's Republic of China
- ⁶¹ University of Groningen, NL-9747 AA Groningen, The Netherlands
- ⁶² University of Hawaii, Honolulu, Hawaii 96822, USA
- ⁶³ University of Jinan, Jinan 250022, People's Republic of China
- ⁶⁴ University of Manchester, Oxford Road, Manchester, M13 9PL, United Kingdom
- ⁶⁵ University of Muenster, Wilhelm-Klemm-Strasse 9, 48149 Muenster, Germany
- ⁶⁶ University of Oxford, Keble Road, Oxford OX13RH, United Kingdom
- ⁶⁷ University of Science and Technology Liaoning, Anshan 114051, People's Republic of China
- ⁶⁸ University of Science and Technology of China, Hefei 230026, People's Republic of China
- ⁶⁹ University of South China, Hengyang 421001, People's Republic of China
- ⁷⁰ University of the Punjab, Lahore-54590, Pakistan
- ⁷¹ University of Turin and INFN, (A)University of Turin, I-10125, Turin, Italy; (B)University of Eastern Piedmont, I-15121, Alessandria, Italy; (C)INFN, I-10125, Turin, Italy
- ⁷² Uppsala University, Box 516, SE-75120 Uppsala, Sweden
- ⁷³ Wuhan University, Wuhan 430072, People's Republic of China
- ⁷⁴ Xinyang Normal University, Xinyang 464000, People's Republic of China
- ⁷⁵ Yantai University, Yantai 264005, People's Republic of China
- ⁷⁶ Yunnan University, Kunming 650500, People's Republic of China
- ⁷⁷ Zhejiang University, Hangzhou 310027, People's Republic of China
- ⁷⁸ Zhengzhou University, Zhengzhou 450001, People's Republic of China
- ^a Also at the Moscow Institute of Physics and Technology, Moscow 141700, Russia
- ^b Also at the Novosibirsk State University, Novosibirsk, 630090, Russia
- ^c Also at the NRC "Kurchatov Institute", PNPI, 188300, Gatchina, Russia
- ^d Also at Goethe University Frankfurt, 60323 Frankfurt am Main, Germany
- ^e Also at Key Laboratory for Particle Physics, Astrophysics and Cosmology, Ministry of Education; Shanghai Key Laboratory for Particle Physics and Cosmology; Institute of Nuclear and Particle Physics, Shanghai 200240, People's Republic of China
- ^f Also at Key Laboratory of Nuclear Physics and Ion-beam Application (MOE) and Institute of Modern Physics, Fudan University, Shanghai 200443, People's Republic of China
- ^g Also at State Key Laboratory of Nuclear Physics and Technology, Peking University, Beijing 100871, People's Republic of China
- ^h Also at School of Physics and Electronics, Hunan University, Changsha 410082, China
- ⁱ Also at Guangdong Provincial Key Laboratory of Nuclear Science, Institute of Quantum Matter, South China Normal University, Guangzhou 510006, China
- ^j Also at Frontiers Science Center for Rare Isotopes, Lanzhou University, Lanzhou 730000, People's Republic of China
- ^k Also at Lanzhou Center for Theoretical Physics, Lanzhou University, Lanzhou 730000, People's Republic of China

^l Also at the Department of Mathematical Sciences, IBA, Karachi , Pakistan

Abstract We report a search for a heavier partner of the recently observed $Z_{cs}(3985)^-$ state, denoted as $Z_{cs}'^-$, in the process $e^+e^- \rightarrow K^+ D_s^{*-} D^{*0} + c.c.$, based on e^+e^- collision data collected at the center-of-mass energies of $\sqrt{s} = 4.661, 4.682$ and 4.699 GeV with the BESIII detector. The $Z_{cs}'^-$ is of interest as it is expected to be a candidate for a hidden-charm and open-strange tetraquark. A partial-reconstruction technique is used to isolate K^+ recoil-mass spectra, which are probed for a potential contribution from $Z_{cs}'^- \rightarrow D_s^{*-} D^{*0}$ (*c.c.*). We find an excess of $Z_{cs}'^- \rightarrow D_s^{*-} D^{*0}$ (*c.c.*) candidates with a significance of 2.1σ , after considering systematic uncertainties, at a mass of $(4123.5 \pm 0.7_{\text{stat.}} \pm 4.7_{\text{syst.}}) \text{ MeV}/c^2$. As the data set is limited in size, the upper limits are evaluated at the 90% confidence level on the product of the Born cross sections (σ^{Born}) and the branching fraction (\mathcal{B}) of $Z_{cs}'^- \rightarrow D_s^{*-} D^{*0}$, under different assumptions of the $Z_{cs}'^-$ mass from 4.120 to 4.140 MeV and of the width from 10 to 50 MeV at the three center-of-mass energies. The upper limits of $\sigma^{\text{Born}} \cdot \mathcal{B}$ are found to be at the level of $\mathcal{O}(1)$ pb at each energy. Larger data samples are needed to confirm the $Z_{cs}'^-$ state and clarify its nature in the coming years.

Key words electron-positron collision, BESIII, hadron spectroscopy, tetraquark

PACS 13.66.Bc, 14.40.Rt, 13.30.Eg

1 Introduction

The many examples of exotic-hadron candidates that have been reported in recent years provide important constraints on Quantum Chromodynamic (QCD) phenomenological models and further deepen our understanding of the strong interaction, offering insights beyond those available through studies of conventional mesons and baryons [1–5]. In 2021, the first observation of a charged hidden-charm tetraquark candidate with strangeness, named $Z_{cs}(3985)^-$, decaying into $D_s^- D^{*0}$ and $D_s^{*-} D^0$, was reported in the process $e^+e^- \rightarrow K^+(D_s^- D^{*0} + D_s^{*-} D^0)$ by the BESIII Collaboration [6]. Here and elsewhere, the charge-conjugation mode is always implied, unless otherwise stated. The mass and width of the $Z_{cs}(3985)^-$ were measured to be $(3982.5^{+1.8}_{-2.6} \pm 2.1) \text{ MeV}/c^2$ and $(12.8^{+5.3}_{-4.4} \pm 3.0) \text{ MeV}$, respectively. The LHCb Collaboration later reported two more charged $Z_{cs}(4000)^-$ and $Z_{cs}(4220)^-$ states in the mass spectra of $J/\psi K^-$ in B decays [7]. These observations have stimulated much theoretical discussion, especially, on the relationship between the $Z_{cs}(3985)^-$, $Z_{cs}(4000)^-$ and $Z_{cs}(4220)^-$ states [1, 8]. One notable observation is that the width of the $Z_{cs}(3985)^-$ is much narrower than those of the $Z_{cs}(4000)^-$ and $Z_{cs}(4220)^-$. This indicates that the $Z_{cs}(3985)^-$ and $Z_{cs}(4000)^-$ may be not the same state, although they are close-lying in mass [9, 10]. Earlier this year, the BESIII Collaboration reported [11] evidence for the neutral $Z_{cs}(3985)^0$ state in the process $e^+e^- \rightarrow K_S^0(D_s^+ D^{*-} + D_s^{*+} D^-)$, whose mass and width are close to those of the charged $Z_{cs}(3985)^-$. Furthermore, the relative Born cross sections for the production of these two states agree with the expectations of isospin symmetry. Hence, the $Z_{cs}(3985)^0$ is regarded as the isospin partner of the $Z_{cs}(3985)^-$ [11].

As discussed in Refs. [12–33], heavier partners of the $Z_{cs}(3985)^-$ might exist, which are denoted as Z'_{cs} . The Z'_{cs} state is expected to decay with large rate to the final state of $D_s^{*-} D^{*0}$, and has masses ranging from 4120 to 4200 MeV/c^2 in different models [18–32]. For example, Z'_{cs} is assumed to be a $D_s^{*-} D^{*0}$ molecule with a mass of 4140 MeV/c^2 in Ref. [18] while the heavy $SU(3)_f$ partner of $Z_{cs}(3985)^-$ is predicted to have a mass of 4124 MeV/c^2 in chiral effective field theory [22]. Thus, it is crucial to search for the Z'_{cs} state and measure its properties to distinguish between these models.

In this paper, we search for Z'_{cs} state in the process of $e^+e^- \rightarrow K^+ D_s^{*-} D^{*0}$, taking advantage of e^+e^- collision data collected with the BESIII detector at

the center-of-mass energies $\sqrt{s} = 4.661, 4.682$, and 4.699 GeV [34]. The corresponding integrated luminosity of these data samples is 2.7 fb^{-1} [34].

2 BESIII detector

The BESIII detector [35] records symmetric e^+e^- collisions provided by the BEPCII storage ring [36] in the center-of-mass energy range from 2.0 to 4.95 GeV , with a peak luminosity of $1 \times 10^{33} \text{ cm}^{-2}\text{s}^{-1}$ achieved at $\sqrt{s} = 3.77 \text{ GeV}$. BESIII has collected many data samples in this energy region [37]. The cylindrical core of the BESIII detector covers 93% of the full solid angle and consists of a helium-based multilayer drift chamber (MDC), a plastic scintillator time-of-flight system (TOF), and a CsI(Tl) electromagnetic calorimeter (EMC), which are all enclosed in a superconducting solenoidal magnet providing a 1.0 T magnetic field. The solenoid is supported by an octagonal flux-return yoke with resistive plate counter muon identification modules interleaved with steel. The charged-particle momentum resolution at 1 GeV/c is 0.5%, and the specific ionization energy loss dE/dx resolution is 6% for electrons from Bhabha scattering. The EMC measures photon energies with a resolution of 2.5% (5%) at 1 GeV in the barrel (end-cap) region. The time resolution of the TOF barrel part is 68 ps, while that of the end-cap part is 110 ps. The end-cap TOF system was upgraded in 2015 using multi-gap resistive plate chamber technology, providing a time resolution of 60 ps [38–40].

3 Monte Carlo simulation

Simulated data samples produced with a GEANT4-based [41] Monte Carlo (MC) package, which includes the geometric description of the BESIII detector [42–44] and the detector responses, are used to determine detection efficiencies and to estimate backgrounds. The simulation models the beam-energy spread and initial-state radiation (ISR) in the e^+e^- annihilations with the generator KKMC [45, 46]. For the three-body non-resonant (NR) signal process, $e^+e^- \rightarrow K^+ D_s^{*-} D^{*0}$, the final-state particles are simulated assuming non-resonant production [37]. For the simulation of the Z'_{cs} signal process, $e^+e^- \rightarrow K^+ Z'_{cs} \rightarrow K^+ D_s^{*-} D^{*0}$, the spin-parity J^P of the Z'_{cs} is assumed to be 1^+ in accordance with Refs. [6, 7], as the corresponding production and subsequent decay process are both dominated by S wave. However, other spin-parity assignments are allowed, and considered in the assignment of systematic uncertainties.

4 Event selection

To ensure a high selection efficiency, we employ a partial-reconstruction method, in which we use two tag modes to identify the process of $e^+e^- \rightarrow K^+ D_s^{*-} D^{*0}$. In the D_s^- -tag mode, we reconstruct the prompt K^+ and the decay products of the D_s^- via the $D_s^- \rightarrow K^+ K^- \pi^+$ or $K_S^0 K^-$ processes. The strategy for the D^{*0} -tag mode is similar to the D_s^- -tag case but here the D^{*0} is reconstructed via $D^{*0} \rightarrow D^0 \pi^0$, and $D^0 \rightarrow K^- \pi^+$ or $K^- \pi^+ \pi^+ \pi^-$, $\pi^0 \rightarrow \gamma\gamma$ process.

Each charged track is required to have a polar angle θ in the range $|\cos\theta| < 0.93$. For all such tracks, apart from those used to construct K_S^0 candidates, the distances of closest approach to the interaction point (V_z) are required to be less than 10 cm along the beam direction and less than 1 cm in the plane perpendicular to the beam (V_r). The dE/dx in the MDC and the time of flight information measured in the TOF are used to calculate particle identification (PID) likelihood values for the pion (\mathcal{L}_π) and kaon (\mathcal{L}_K) hypotheses. Pion candidates are selected by requiring $\mathcal{L}_\pi > \mathcal{L}_K$, and kaon candidates are required to satisfy $\mathcal{L}_K > \mathcal{L}_\pi$.

Photon candidates are reconstructed from isolated clusters in the EMC in the regions $|\cos\theta| \leq 0.80$ (barrel) or $0.86 \leq |\cos\theta| \leq 0.92$ (end cap). The deposited energy of a cluster is required to be greater than 25 (50) MeV in the barrel (end-cap) region. To suppress electronic noise and energy deposits unrelated to the events, the difference between the EMC time and the event start time is required to be within (0, 700) ns. The π^0 candidates are reconstructed from all combinations of photon pairs and the diphoton invariant mass, $M_{\gamma\gamma}$, is required to satisfy $0.115 < M_{\gamma\gamma} < 0.150$ GeV/ c^2 .

Candidates for K_S^0 mesons are reconstructed from two oppositely charged tracks, with no PID requirement; A looser requirement of $V_z < 20$ cm is applied on these tracks than $R_z < 10$ cm while no V_r requirement is applied. Furthermore, there is usually a detectable displacement before the decay of K_S^0 meson due to its relatively long lifetime. Therefore, the decay length and corresponding uncertainty of K_S^0 candidates are required to satisfy $L/\sigma_L > 2$, which suppresses the prompt $\pi^+\pi^-$ combinatorial background [47]. The K_S^0 meson candidates that lie within the invariant-mass window $0.485 < M(\pi^+\pi^-) < 0.511$ GeV/ c^2 are retained.

The D_s^- and D^{*0} candidates for all decay modes are reconstructed by considering all combinations of selected charged track, π^0 and K_S^0 candidates. To

improve the signal purity in the selected $D_s^- \rightarrow K^+ K^- \pi^-$ candidates, we only retain the D_s^- formed by $D_s^- \rightarrow \phi\pi^-$ or $D_s^- \rightarrow K^*(892)^0 K^-$ by requiring $M(K^+ K^-) < 1.05$ GeV/ c^2 or $0.850 < M(K^+ \pi^-) < 0.930$ GeV/ c^2 . Figure 1 shows the invariant mass spectra of the D_s^- and D^0 candidates at $\sqrt{s} = 4.682$ GeV, in which the signal peaks are clearly evident. To select the D_s^- and D^0 signal candidates, their reconstructed invariant masses are restricted to lie in the regions (1.955, 1.980) GeV/ c^2 and (1.850, 1.880) GeV/ c^2 , respectively. Furthermore, in the selection of $D^{*0} \rightarrow D^0 \pi^0$ decays, the invariant mass of the D^0 and π^0 candidate, $M(D^0 \pi^0)$, is calculated with the reconstructed momenta of the final states and the known $m(\pi^0)$ mass from the PDG [48] in order to improve mass resolution [49], as shown in Fig. 1. In case there are multiple D^{*0} candidates per event, only the candidate with invariant mass in the region (2.000, 2.014) GeV/ c^2 and closest to the known D^{*0} mass is kept.

Figure 2 shows the spectrum of the $K^+ D_s^-$ ($K^+ D^{*0}$) recoil mass, $RM(K^+ D_s^-)$ ($RM(K^+ D^{*0})$), for the D_s^- (D^{*0}) candidate events from the data samples at $\sqrt{s} = 4.682$ GeV. Here, $RM(X) = \|p_{e^+e^-} - p_X\|$, where $p_{e^+e^-}$ is the four-momentum of the initial e^+e^- system and p_X is the four-momentum of the system X . The $RM(K^+ D_s^-)$ ($RM(K^+ D^{*0})$) is corrected by substituting the reconstructed D_s^- (D^{*0}) mass with the known mass $m(D_s^-)$ ($m(D^{*0})$) from the PDG [48]. In the $RM(K^+ D_s^-)$ spectrum with the D_s^- -tag method shown in Fig. 2, the peak around the mass of D^{*0} of 2006.85 MeV/ c^2 [48] is due to background process $e^+e^- \rightarrow K^+ D_s^{*-} D^{*0}$. The process $e^+e^- \rightarrow K^+ D_s^{*-} D^0$ also contributes to this peak but shows a broader structure. These processes will not dilute the enhancement above 2.11 GeV/ c^2 corresponding to the combination of the unreconstructed D^{*0} and γ (π^0) from the D_s^{*-} decays in the signal process $e^+e^- \rightarrow K^+ D_s^{*-} D^{*0}$. Based on this feature, we further improve the signal purity with the requirement $R(K^+ D_s^-) > 2.11$ GeV/ c^2 . In the D^{*0} -tag method, a clear peak is seen in the $RM(K^+ D^{*0})$ spectrum at the nominal D_s^{*-} mass. Therefore, we require $RM(K^+ D^{*0})$ to be in the interval (2.102, 2.122) GeV/ c^2 to isolate the D_s^{*-} signals. The double-counting rate between these two tag methods is negligible after applying all the above selection criteria. The resulting $RM(K^+)$ spectra for the surviving events at various energy points, as shown in Fig. 3, are then probed for contributions from the Z_{cs}^{*-} state. Estimated background processes are also overlaid in Fig. 3.

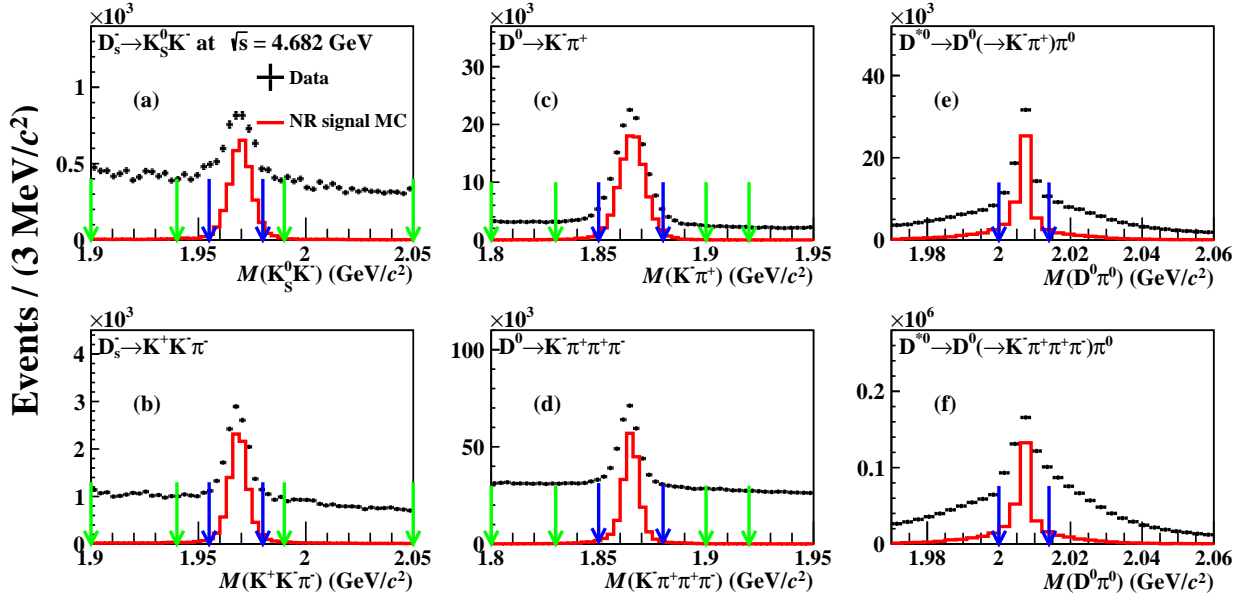


Figure 1. The (a) $K^+K^-\pi^-$, (b) $K_S^0K^-$, (c) $K^-\pi^+$, (d) $K^-\pi^+\pi^+\pi^-$ invariant-mass spectra and (e,f) the corresponding $D^0\pi^0$ mass spectra. The black dots are the data sample at $\sqrt{s} = 4.682$ GeV, the red histograms are the NR signal MC samples, and the blue (green) arrows indicate the signal (sideband) regions.

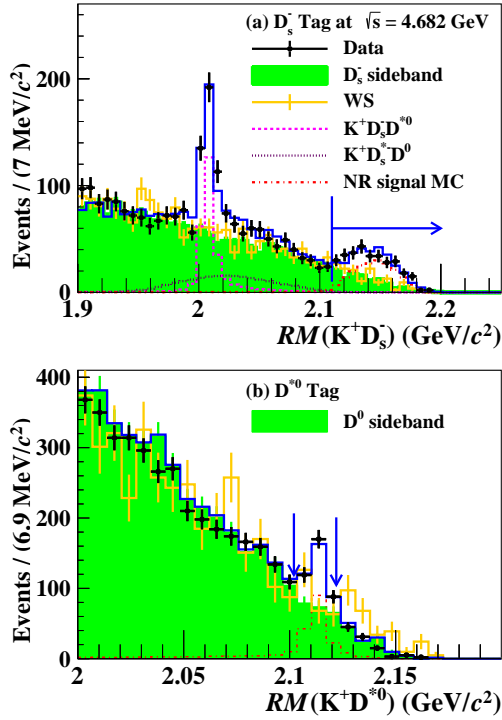


Figure 2. The spectra of (a) recoil mass $RM(K^+D_s^-)$ of $K^+D_s^-$ and (b) recoil mass $RM(K^+D^{*0})$ of K^+D^{*0} for the $D_s^-(D^{*0})$ candidate events at $\sqrt{s} = 4.682$ GeV. The scaled background control samples of wrong sign (WS) events and $D_{(s)}$ sideband events are overlaid to represent the combinatorial backgrounds. The scaled NR signal MC is also overlaid. The blue lines are the sum of spectra of scaled D_s^- sideband, $e^+e^- \rightarrow K^+D_s^-D^{*0}$

and $e^+e^- \rightarrow K^+D_s^{*-}D^0$ and NR signal MC. The blue arrows indicate the selected region for the $e^+e^- \rightarrow K^+D_s^{*-}D^{*0}$ candidates.

The combinatorial background shape is derived from the kernel estimation [50] of a mixed background sample formed from wrong-sign (WS) combinations and $D_s^-(D^0)$ mass sideband events. The WS sample consists of K^- and $D_s^-(\bar{D}^{*0})$ combinations, rather than the right-sign K^+ and $D_s^-(\bar{D}^{*0})$ combinations for the correct signal selection. The sideband samples for the D_s^- and D^0 events are defined as $(1.90, 1.94) \parallel (1.99, 2.05)$ GeV/ c^2 in the D_s^- invariant-mass spectrum, and $(1.80, 1.83) \parallel (1.90, 1.92)$ GeV/ c^2 in the D^0 invariant-mass spectrum, as depicted in Fig. 1. When forming the mixed background sample, we scale the contribution of the $D_s^-(D^0)$ mass sideband events to equal that of the WS combinations. The number of background events within the signal region is estimated by a fit to the $RM(K^+D_s^-)$ ($RM(K^+D^{*0})$) spectrum of the sideband events with the shape extracted from the mixed sample, as described in Ref. [11]. In the fit to the $RM(K^+D_s^-)$ spectrum, two additional contributions from the processes $e^+e^- \rightarrow K^+D_s^-D^{*0}$ and $K^+D_s^{*-}D^0$ are taken into account, whose shapes are derived from MC simulations. Table 1 lists the numbers of combinatorial background events in Fig. 3 for the two tag methods at various energy points.

Studies are performed with MC simulation to un-

Table 1. Estimated contributions from the combinatorial background and $D_s^{*-}D_{s1}(2536)^+$ events in the final sample of $e^+e^- \rightarrow K^+D_s^{*-}D^{*0}$ candidates for the two tag methods at various energy points. The uncertainties are statistical.

Background source	Tag	4.661 GeV	4.682 GeV	4.699 GeV
Comb. bkg	D_s^- -tag	27 ± 5	120 ± 11	54 ± 7
	D^{*0} -tag	33 ± 6	216 ± 15	103 ± 10
$D_s^{*-}D_{s1}(2536)^+$	D_s^- -tag	18 ± 7	117 ± 27	52 ± 13
	D^{*0} -tag	15 ± 6	91 ± 21	33 ± 9

derstand the potential contributions to the $RM(K^+)$ spectra from the excited charmed mesons $D_{(s)}^{**}$, *i.e.*, $e^+e^- \rightarrow D_s^{*-}D_s^{**+}(\rightarrow D^{*0}K^+)$ or $D^{*0}D^{**0}(\rightarrow D_s^{*-}K^+)$, which have the same final states as the signal processes. These studies account for all known $D_{(s)}^{**}$ states [48, 51]. It is found that the channel $e^+e^- \rightarrow D_s^{*-}D_{s1}(2536)^+(\rightarrow D^{*0}K^+)$ gives a broad contribution at the higher mass region in the $RM(K^+)$ spectra, as shown in Fig. 3. We evaluate the size of this contribution according to the measured production cross sections [52], to yield the numbers listed in Table 1. Other potential $D_{(s)}^{**}$ contributions behave in a similar way as the NR signal processes.

As shown in Fig. 3, there is a non-trivial structure around $4.125 \text{ GeV}/c^2$ in the $RM(K^+)$ spectra when excluding the contributions from combinatorial backgrounds and $D_s^{*-}D_{s1}(2536)^+$ components. Both the D_s^- -tag and D^{*0} -tag samples show an enhancement above the estimated backgrounds and the NR process, in particular at $\sqrt{s} = 4.682 \text{ GeV}$.

5 Measurement of resonance parameters

We consider the enhancement around $4.125 \text{ GeV}/c^2$ in the $RM(K^+)$ spectra to be a $D_s^{*-}D^{*0}$ resonance, which we denote as $Z_{cs}'^-$. To estimate the number of $Z_{cs}'^-$ events in the sample, we perform a simultaneous unbinned maximum-likelihood fit to the $RM(K^+)$ spectra for the three energy points with the two tag methods, as shown in Fig. 3. The $Z_{cs}'^-$ component is modeled with an efficiency-weighted Breit-Wigner function convolved with a resolution function estimated from MC simulations. The Breit-Wigner function assumes an S -wave in the following form

$$\mathcal{F}(M) \propto \left| \frac{\sqrt{q \cdot p}}{M^2 - m_0^2 + im_0\Gamma(M)} \right|^2,$$

with $\Gamma(M) = \Gamma_0 \cdot \frac{p}{p^*} \cdot \frac{m_0}{M}$. Here, M is the reconstructed mass, m_0 is the resonance mass, Γ_0 is the width, q is the K^+ momentum in the initial e^+e^- system, p is the D_s^{*-} momentum in the rest frame of the $D_s^{*-}D^{*0}$ system, and p^* is the D_s^{*-} momentum in the rest frame of the $D_s^{*-}D^{*0}$ system at $M = m_0$. The resolution is about $4(8) \text{ MeV}/c^2$ for $D^{*0}(D_s^-)$ -tag and is asymmetric due to ISR effects. The resolution in D^{*0} -tag method is less affected by ISR effects than the D_s^- -tag method. More events that emit ISR photons are removed in the D^{*0} -tag method by the tighter signal window of $RM(K^+D^{*0})$ defined in Fig 2. Thus, the resolution in the D^{*0} -tag method becomes better than that in D_s^- -tag method. The parameterization of the combinatorial-background shape is derived from the kernel estimate [50] of the mixed-background samples, which have been normalized to the estimated numbers as listed in Table 1. The components of the NR signals and $D_s^{*-}D_{s1}(2536)^+$ are included with shapes derived from MC simulations. The sizes of the NR signals are free parameters in the fit, while the contributions from $D_s^{*-}D_{s1}(2536)^+$ are fixed to the numbers in Table 1.

From the simultaneous fit, the mass of $Z_{cs}'^-$ is determined to be $m_0 = (4123.5 \pm 0.7) \text{ MeV}/c^2$. The statistical significance of the signal is 3.9σ , which is calculated with 5 degrees of freedom and $-2\ln(L_0/L_{\max}) = 25.8$, where L_0 and L_{\max} are the fitted likelihood values with and without involving the $Z_{cs}'^-$ signal component in the fit, respectively. The degrees of freedom consist of the signal yields at the three center-of-mass energies and the mass and width of the $Z_{cs}'^-$ state. After taking into account the systematic uncertainties, the significance is reduced to 2.1σ . The width Γ_0 is not reported as the size of the data samples is inadequate to determine this parameter in the fit. Alternatively, we perform a series of local p -value scans under different width assumptions (10, 20, 30, 40, 50) MeV in the $RM(K^+)$ spectra, as shown in Fig. 6. The minimum p -value is found to be 4.0×10^{-5} at $m_0 = 4124.1 \text{ MeV}/c^2$ with

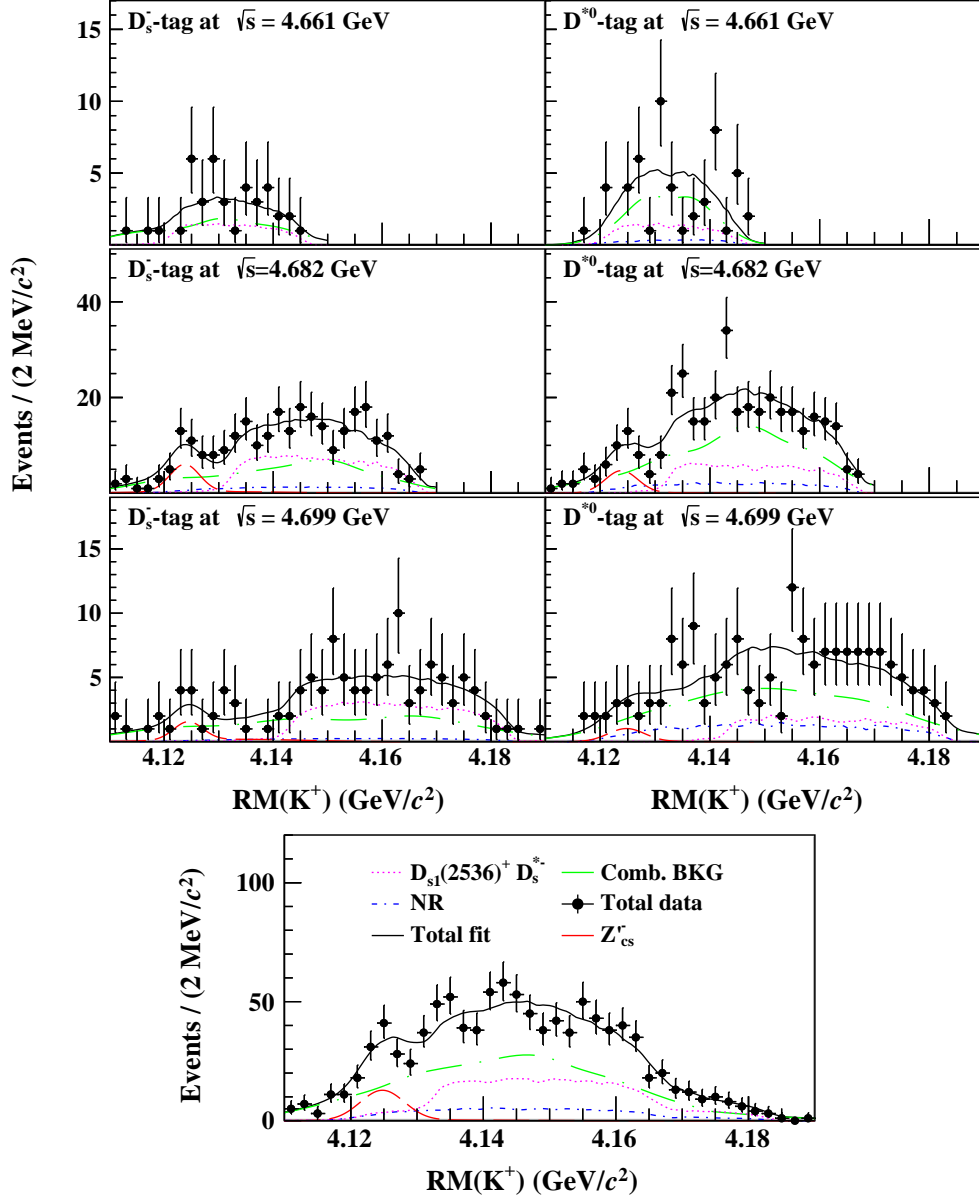


Figure 3. The spectra of K^+ recoil mass from D^{*-} - and D_s^{*-} -tag methods after all selection criteria at $\sqrt{s} = 4.661, 4.682$ and 4.699 GeV. The simultaneous fit results are overlaid, where the red dashed lines are Z_{cs}' signals, the blue dashed-dotted lines are NR processes, the green dashed-dotted lines are combinatorial background, the purple dashed lines represent the process $e^+e^- \rightarrow D_s^{*-} D_{s1}(2536)^+$ and the black solid lines are the sum of all components.

Table 2. The fitted Z'_{cs} yields (N_{obs}), the detection efficiencies ($\hat{\varepsilon}$), the integrated luminosities (\mathcal{L}^{int}), the vacuum polarization correction factors ($1 + \delta_{\text{VP}}$) and the results for $\sigma^{\text{obs}} \cdot \mathcal{B}$ for the different energy points. The uncertainties are statistical only.

\sqrt{s} (GeV)	Tag	N_{obs}	$\hat{\varepsilon}$ (%)	\mathcal{L}^{int} (pb $^{-1}$)	$(1 + \delta_{\text{VP}})$	$\sigma^{\text{obs}} \cdot \mathcal{B}$ (pb)
4.661	D_s^- -tag	$0_{-0}^{+1.7}$	0.1578 ± 0.0009	529.63	1.055	$0.0_{-0.0}^{+0.3}$
	D^{*0} -tag	$0_{-0}^{+1.3}$	0.0293 ± 0.0004			
4.682	D_s^- -tag	25_{-7}^{+7}	0.2017 ± 0.0009	1669.31	1.055	$1.2_{-0.3}^{+0.3}$
	D^{*0} -tag	18_{-5}^{+5}	0.0363 ± 0.0004			
4.699	D_s^- -tag	7_{-4}^{+5}	0.2151 ± 0.0009	536.45	1.055	$0.9_{-0.5}^{+0.6}$
	D^{*0} -tag	$4.6_{-2.6}^{+3.1}$	0.0347 ± 0.0004			

Table 3. The upper limits for $\sigma_{\text{upper}}^{\text{Born}} \cdot \mathcal{B}$ in unit of pb at the 90% confidence level at $\sqrt{s} = 4.661, 4.682$, and 4.699 GeV. Here, both statistical and systematic uncertainties are taken into account.

$m_0(Z'_{cs})$ (MeV/ c^2)	$\Gamma_0 = 10$ MeV	$\Gamma_0 = 20$ MeV	$\Gamma_0 = 30$ MeV	$\Gamma_0 = 40$ MeV	$\Gamma_0 = 50$ MeV
at $\sqrt{s} = 4.661$ GeV					
4120	1.8	1.9	1.9	2.0	2.0
4125	2.8	2.6	2.6	3.4	2.4
4130	4.0	3.8	3.5	3.2	2.9
4135	3.7	4.0	4.1	5.6	4.0
4140	4.4	4.0	4.2	4.3	4.3
at $\sqrt{s} = 4.682$ GeV					
4120	3.3	3.6	3.7	3.8	3.8
4125	4.5	4.7	4.9	4.9	4.8
4130	4.3	5.0	5.2	5.2	5.2
4135	3.9	5.5	6.2	6.3	6.3
4140	2.8	4.5	5.8	6.4	6.6
at $\sqrt{s} = 4.699$ GeV					
4120	4.1	4.8	4.9	5.0	5.0
4125	5.1	5.3	5.6	5.7	5.8
4130	4.1	4.5	4.9	5.2	5.2
4135	4.4	5.2	5.7	6.1	6.1
4140	2.7	3.8	4.6	5.4	5.4

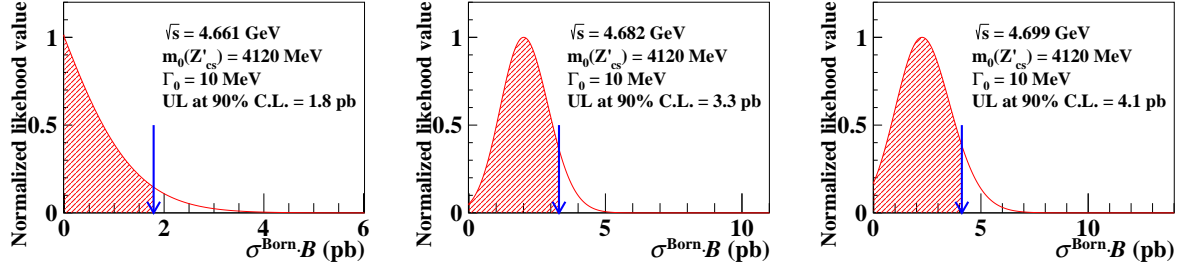


Figure 4. Likelihood scan of $\sigma^{\text{Born}} \cdot \mathcal{B}$ for the data samples at $\sqrt{s} = 4.661, 4.682$, and 4.699 GeV after considering systematic uncertainties. The blue arrow indicates the upper limit at the 90% confidence level. In the likelihood scan, the PDFs which result in the largest upper limits are used, and the mass and width of Z'_{cs} are fixed to $4120 \text{ MeV}/c^2$ and 10 MeV , respectively.

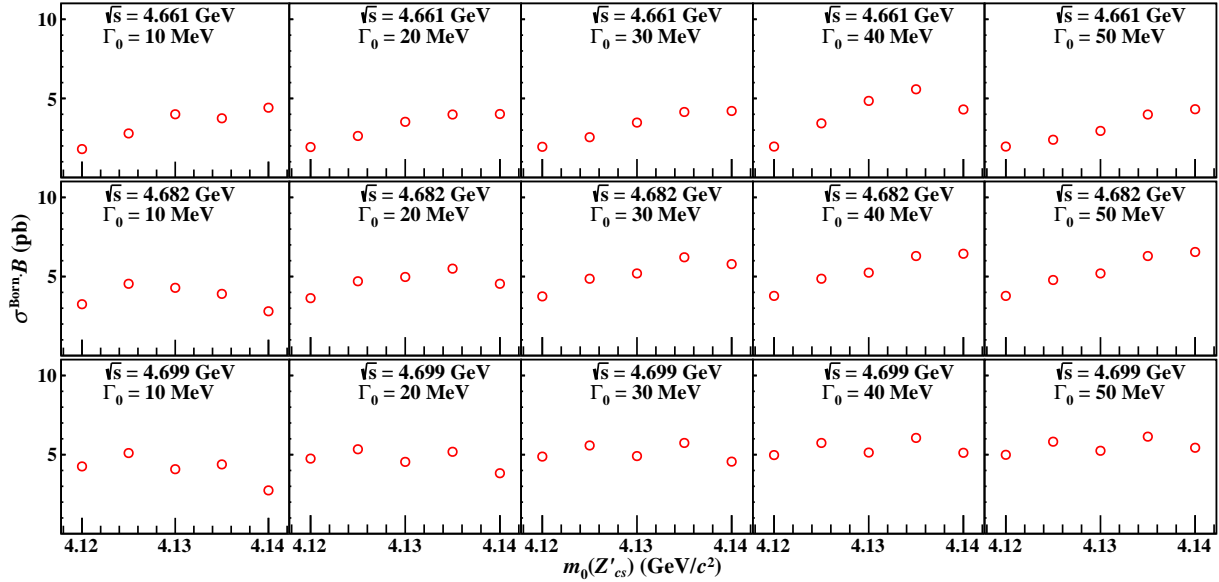


Figure 5. Upper limits (open red circles) for $\sigma^{\text{Born}}_{\text{upper}} \cdot \mathcal{B}$ at the 90% confidence level for the assumed masses of $m_0(Z'_{cs}) = 4120, 4125, 4130, 4135$ and $4140 \text{ MeV}/c^2$, and the assumed widths of $\Gamma_0 = 10, 20, 30, 40$ and 50 MeV at $\sqrt{s} = 4.661, 4.682$ and 4.699 GeV.

$\Gamma_0 = 10 \text{ MeV}$, corresponding to a local statistical significance of 4.1σ .

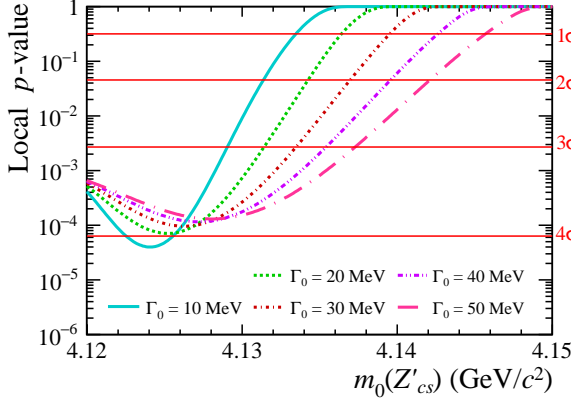


Figure 6. The local p -value as a function of $m_0(Z'_{cs})$ from the simultaneous fit to data samples at $\sqrt{s} = 4.661, 4.682$, and 4.699 GeV .

6 Measurement of Born cross sections

The product of the Born cross section and the branching fraction of $Z'_{cs} \rightarrow D_s^{*-} D^{*0}$, $\sigma^{\text{Born}}(e^+e^- \rightarrow K^+ Z'_{cs} + c.c.) \cdot \mathcal{B}(Z'_{cs} \rightarrow D_s^{*-} D^{*0})$ ($\sigma^{\text{Born}} \cdot \mathcal{B}$ for short), is determined by

$$\sigma^{\text{Born}} \cdot \mathcal{B} = \frac{N_{\text{obs},i}^k}{\mathcal{L}_i^{\text{int}} \cdot \hat{\varepsilon}_i^k \cdot (1 + \delta_{\text{ISR}})_i \cdot (1 + \delta_{\text{VP}})_i}. \quad (1)$$

Here $N_{\text{obs},i}^k$ is the Z'_{cs} signal yield from the fit shown in Fig. 3; $\hat{\varepsilon}_i^k$ is the combined branching-fraction-weighted detection efficiency in different $D_s^-(D^{*0})$ decay modes; $\mathcal{L}_i^{\text{int}}$ is the integrated luminosity; $(1 + \delta_{\text{ISR}})_i$ is the ISR correction factor; $(1 + \delta_{\text{VP}})_i$ is the vacuum-polarization correction factor, which is calculated according to Ref. [53]; and i and k denote the energy point ($1 \leq i \leq 3$) and tag method ($1 \leq k \leq 2$), respectively. The measured values of $\sigma^{\text{obs}} \cdot \mathcal{B}$ are listed in Table 2.

We furthermore determine the upper limits of $\sigma^{\text{Born}} \cdot \mathcal{B}$ at the 90% confidence level at all three energy points for different values of the Z'_{cs} mass and width by measuring the signal yields under these different assumptions. The upper limits are obtained via a likelihood scan, as illustrated in Fig. 4. The systematic uncertainties are taken into account in the upper-limit estimation by adopting a Gaussian constraint method [54] in the likelihood scan. Here, to be conservative, the ISR correction factor $(1 + \delta_{\text{ISR}})_i$ are evaluated based on a hypothetical narrow resonant line shape of the cross sections with a width of 10 MeV following the method in Ref. [55], which gives a minimum ISR correction factor. The ISR correction

factors as a function of \sqrt{s} is shown in Fig. 7. The upper limits of $\sigma^{\text{Born}} \cdot \mathcal{B}$ after accounting for systematic uncertainties are shown in Fig. 5 and Table 3.

7 Systematic uncertainty

The systematic uncertainties on the mass measurement of the Z'_{cs} and the upper-limit cross sections are summarized in Table 4 and Table 5, respectively. For the mass measurement, the systematic uncertainties are mainly from the estimation of combinatorial background and the $D_s^{*-} D_{s1}(2536)^+$ contribution, the input Born cross-section line shape for $\sigma^{\text{Born}}(e^+e^- \rightarrow K^+ Z'_{cs})$, detector resolution, mass scaling and signal model. These sources of uncertainty are augmented by additional contributions in the cross-section measurement.

7.1 Systematic uncertainties on the mass measurement

Table 4. Absolute systematic uncertainties in the measurement of the Z'_{cs} mass.

Source	Mass (MeV/c^2)
Comb. background	0.1
$D_s^{*-} D_{s1}(2536)^+$	0.1
$\sigma^{\text{Born}}(e^+e^- \rightarrow K^+ Z'_{cs})$ line shape	0.5
Signal model	0.1
Mass scaling	0.5
Resolution	0.8
Efficiency curve	< 0.1
Γ_0 assumptions	4.6
Total	4.7

The systematic uncertainties related to the combinatorial backgrounds and $D_s^{*-} D_{s1}(2536)^+$ contributions are estimated by floating their sizes with a Gaussian constraint in the fit. The mean and width of the Gaussian function are derived according to the estimated yields and the corresponding uncertainties, as listed in Table 1. Both show variation of $0.1 \text{ MeV}/c^2$ on the fitted mass, which is taken as the systematic uncertainty.

We replace the input Born cross-section line shape of $\sigma^{\text{Born}}(e^+e^- \rightarrow K^+ Z'_{cs})$ in MC production with a narrow Breit-Wigner line-shape assumption and repeat the signal determination. The width of the narrow Breit-Wigner line-shape is chosen to be 10 MeV , which is much narrower than the nominal. The

change of $0.5 \text{ MeV}/c^2$ for the fitted mass is assigned as the systematic uncertainty.

In the nominal fit, the signal model is based on the spin-parity assumption of Z'_{cs} as $J^P = 1^+$ and the assumption that the relative momentum between K^+ and Z'_{cs} in the rest frame of the e^+e^- system and the relative momentum between D_s^{*-} and D^{*0} in the Z'_{cs} system are both in an S -wave state, denoted as $1^+(S, S)$. These assumptions are consistent with the study of $Z_{cs}(3985)^-$ [6]. As systematic variations, we examine the assumptions of spin-parity and angular momentum with $0^-(P, P), 1^-(P, P), 1^+(D, S), 2^-(P, P)$ and $2^+(D, S)$ configurations. The maximum change of $0.1 \text{ MeV}/c^2$ for the fitted mass is assigned as the systematic uncertainty for the spin-parity assumption.

We select a control sample of $e^+e^- \rightarrow D_s^{*-} D_{s1}(2536)^+$, as done in Ref. [6], to study the mass scaling of the recoil mass of the low-momentum bachelor K^+ . An MC-determined signal shape convolved with a Gaussian function is used to represent the difference between data and MC simulation. The mean and width of this function are determined to be $-0.2 \pm 0.5 \text{ MeV}/c^2$ and $< 1.43 \text{ MeV}/c^2$ (68% confidence level), respectively. We take the maximum mass shift of $\sqrt{0.2^2 + 0.5^2} \approx 0.5 \text{ MeV}/c^2$ as the systematic uncertainty due to the mass scaling.

To estimate systematic uncertainties associated with resolution smearing function, which reflects imperfect MC simulation for the resolution, we smear the resolution function in the fit to the Z'_{cs} spectrum and re-perform the mass fit. The mean and width of the Gaussian smearing function are also determined from the control sample of $e^+e^- \rightarrow D_s^{*-} D_{s1}(2536)^+$, which are $0.5 \text{ MeV}/c^2$ and $1.43 \text{ MeV}/c^2$. The resultant change in the fitted mass, $0.8 \text{ MeV}/c^2$, is taken as the systematic uncertainty.

The change in the fitted mass is found to be negligible when the efficiency curves adopted in the resonance fit are varied within the uncertainties of their parametrizations.

As previously mentioned, we perform a series of scans under different width assumptions since the Γ_0 of the Z'_{cs} state is not determined due to the limited size of the data samples. Under different width assumptions, the fitted mass can be different. Thus, we assign a systematic uncertainty, $4.6 \text{ MeV}/c^2$, on the measured mass according to the largest discrepancy between the nominal fit result and the fitted mass with the width fixed to the assumed widths.

7.2 Systematic uncertainties on the upper-limit cross sections

We consider three categories of systematic uncertainties on the upper limit of $\sigma_{\text{upper}}^{\text{Born}} \cdot \mathcal{B}$.

Category I includes items such as the detection efficiency, the integrated luminosities and the input branching fractions, whose uncertainties affect the cross-section measurement multiplicatively. Average uncertainties associated with the tracking, PID and $K_S^0(\pi^0)$ reconstruction efficiencies are estimated to be 3.6%, 3.6% and 0.4% (4.1%, 4.1% and 2.0%) in $D_s^-(D^{*0})$ -tag method, respectively. The efficiency of the $RM(K^+ D_s^-)$ and $RM(K^+ D^{*0})$ requirement is re-estimated by changing the MC-simulated resolution according to the observed difference with respect to data. The resulting changes, 0.2% in the D_s^- -tag method, and 6.1%, 5.1% and 4.3% in the D^{*0} -tag method, at various energy points are taken as the systematic uncertainties. The differences in systematic uncertainties here are due to that the requirement of $RM(K^+ D^{*0})$ is much tighter than $RM(K^+ D^{*0})$, which makes the D^{*0} method more sensitive to the resolution changes. The integrated-luminosity uncertainty, measured with large-angle Bhabha scattering events, is estimated to be 1%. The uncertainties on the cited branching fractions for the processes in the reconstructed decay chains are evaluated [48]. The total multiplicative uncertainty is obtained by adding the uncertainties of all these components in quadrature. In the estimation of the upper limit, the multiplicative uncertainty is taken into account through one single Gaussian constraint on the product of the central value of the multiplicative components.

Category II comprises the combinatorial background and $D_s^{*-} D_{s1}(2536)^+$ uncertainties, whose shapes and sizes are fixed in the nominal fit. The uncertainties on their sizes, as listed in Table 1, affect the estimation of the upper limit of $\sigma_{\text{upper}}^{\text{Born}} \cdot \mathcal{B}$. To take into account their effects, the sizes of these contributions are floated in the upper-limit estimation with Gaussian constraints on their uncertainties [54]. In addition, to consider the effects from the background-shape parametrization, a bootstrap resampling method is carried out to generate 500 background toy samples. The background template shape from each toy sample is adopted in each new fit and the distribution of the corresponding differences from the nominal fit is parameterized by a Gaussian function. The likelihood-scan curves are smeared with this Gaussian function to include the systematic effect.

Table 5. Relative systematic uncertainties in the measurement of $\sigma^{\text{Born}} \cdot \mathcal{B}$. The horizontal dividing lines separate the three categories that are described in the main text.

Source	D_s^- -tag			D^{*0} -tag		
	4.661 GeV	4.682 GeV	4.699 GeV	4.661 GeV	4.682 GeV	4.699 GeV
Tracking	3.6%	3.6%	3.6%	4.1%	4.1%	4.1%
PID	3.6%	3.6%	3.6%	4.1%	4.1%	4.1%
$K_S^0(\pi^0)$ reconstruction	0.4%	0.4%	0.4%	2.0%	2.0%	2.0%
$RM(K^+D_s^-(D^{*0}))$	0.2%	0.2%	0.2%	6.1%	5.1%	4.3%
Luminosity	1.0%	1.0%	1.0%	1.0%	1.0%	1.0%
Input branching fractions	2.3%	2.3%	2.3%	1.0%	1.0%	1.0%
Comb. bkg	See Table 1 for the background components.					
$D_s^{*-}D_{s1}(2536)^+$						
Efficiency curve	See main text for discussion of the treatment of these four systematic effects.					
Line shape						
Resolution						
Signal model						

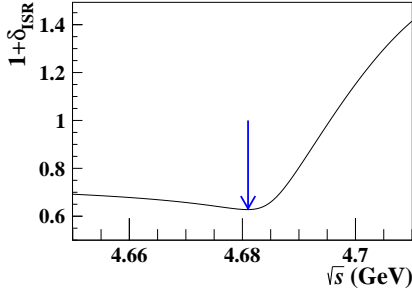


Figure 7. The corresponding ISR correction factor $(1 + \delta_{\text{ISR}})$ as a function of \sqrt{s} for a narrow resonant line shape. We take the minimum of $(1 + \delta_{\text{ISR}})$, as indicated by the blue arrow, to obtain a conservative estimation of $\sigma_{\text{upper}}^{\text{Born}} \cdot \mathcal{B}$.

Category III comprises other sources of uncertainty, such as the efficiency parametrization, the input line shape of the cross sections, the detector resolution and the signal model, for which we evaluate the size of possible bias directly by repeating the fit under different assumptions. The effect from the efficiency parametrization is estimated by varying the parametrization within its fit uncertainties, and the differences in cross sections at each energy point are taken as the corresponding systematic uncertainty. Following Ref. [55], we consider the influence from the input line shape on the estimation of the ISR correction factors by choosing a minimum value of $(1 + \delta_{\text{ISR}})$, as shown in Fig. 7, under a narrow reso-

nant line shape assumption. This provides a conservative estimation on the upper limit. For the resolution effect, we increase the width of the smearing function by 1.43 MeV, which is estimated based on the control sample of $e^+e^- \rightarrow D_s^{*-}D_{s1}(2536)^+$ events as previously mentioned, to accommodate potential differences in the detector resolution between data and MC simulation. For the signal model, we obtain various upper limits of $\sigma_{\text{upper}}^{\text{Born}} \cdot \mathcal{B}$ based on six different spin-parity assignments, as considered for the mass measurement. For all the above variations, the maximum upper limits, after considering the systematic uncertainties of categories I and II, are assigned as the final results for the different resonance parameter hypotheses at the various energy points. The upper limits of $\sigma^{\text{Born}} \cdot \mathcal{B}$, after taking account of the systematic uncertainties, are shown in Fig. 5 and Table 3.

7.3 Systematic uncertainties on the signal significance

The systematic uncertainties on the determination of the signal significance arise from the estimation of combinatorial background and $D_s^{*-}D_{s1}(2536)^+$ contribution, the choice of signal model and the width assumptions. In each signal model aforementioned, we change the fixed sizes of combinatorial background and $D_s^{*-}D_{s1}(2536)^+$ contribution by $\pm 1\sigma$ and then calculate the significance by performing the fits with and without signal components. We adopt 2.1σ , which is the smallest sig-

nificance observed from this procedure, to constitute the result including systematic uncertainties.

8 Summary

Motivated by the observation of $Z_{cs}(3985)^-$, we search for its highly excited partner Z'_{cs} based on the e^+e^- annihilation data collected at $\sqrt{s} = 4.661, 4.682$ and 4.699 GeV with the BESIII detector. By using a partial-reconstruction technique, the K^+ recoil mass spectra are used to search for the Z'_{cs} state in $D_s^{*-}D^{*0}$ events. We find a small excess of $Z'_{cs} \rightarrow D_s^{*-}D^{*0}$ events with a significance of 2.1σ , after considering systematic uncertainties, and measure its mass to be $m_0(Z'_{cs}) = (4123.5 \pm 0.7_{\text{stat.}} \pm 4.7_{\text{syst.}}) \text{ MeV}/c^2$ from a simultaneous fit to all data samples. However, our data set is too small in size to make a meaningful measurement of the width of this state. Hence, a series of Z'_{cs} width hypotheses are tested and the corresponding p -values are evaluated, as shown in Fig. 6. A local min-

imum p -value for Z'_{cs} is found at $m_0 = 4124.1 \text{ MeV}/c^2$ when setting $\Gamma_0 = 10 \text{ MeV}$, corresponding to a local statistical significance of 4.1σ .

Due to the limited sample size, we report the upper limits at the 90% confidence level of the product of the Born cross sections and the branching fraction of the decays $\sigma^{\text{Born}}(e^+e^- \rightarrow K^+Z'_{cs} + c.c.) \cdot \mathcal{B}(Z'_{cs} \rightarrow D_s^{*-}D^{*0})$ at $\sqrt{s} = 4.661, 4.682$, and 4.699 GeV. The search is performed with the mass of Z'_{cs} assumed to be $4.120, 4.125, 4.130, 4.135$ and $4.140 \text{ GeV}/c^2$, and the width assumed to be $10, 20, 30, 40$ and 50 MeV . The upper limits are $2 \sim 6, 3 \sim 7$ and $3 \sim 6 \text{ pb}$ for $\sqrt{s} = 4.661, 4.682$, and 4.699 GeV, respectively, as shown in Fig. 5 and Table 3. The limited statistical precision prevents the establishment of the potential Z'_{cs} state, but the further data taking foreseen in the region $\sqrt{s} = 4.6 \sim 4.9 \text{ GeV}$ [37] may allow for a clearer picture to emerge.

The BESIII collaboration thanks the staff of BEPCII and the IHEP computing center for their strong support.

References

- 1 H. X. Chen, W. Chen, X. Liu, Y. R. Liu, and S. L. Zhu, Rept. Prog. Phys. **86**, 026201 (2023)
- 2 N. Brambilla, S. Eidelman, C. Hanhart, A. Nefediev, C. P. Shen, C. E. Thomas, A. Vairo, and C. Z. Yuan, Phys. Rept. **873**, 1 (2020)
- 3 F. K. Guo, C. Hanhart, U. G. Meißner, Q. Wang, Q. Zhao, and B. S. Zou, Rev. Mod. Phys. **90**, 015004 (2018)
- 4 H. X. Chen, W. Chen, X. Liu, and S. L. Zhu, Phys. Rept. **639**, 1 (2016)
- 5 N. Brambilla *et al.*, Eur. Phys. J. C **71**, 1534 (2011)
- 6 M. Ablikim *et al.* (BESIII Collaboration), Phys. Rev. Lett. **126**, 102001 (2021)
- 7 R. Aaij *et al.* (LHCb Collaboration), Phys. Rev. Lett. **127**, 082001 (2021)
- 8 M. Karliner and J. L. Rosner, Sci. Bull. **66**, 2045 (2021)
- 9 L. Maiani, A. D. Polosa, and V. Riquer, Sci. Bull. **66**, 1616 (2021)
- 10 L. Meng, B. Wang, G. J. Wang, and S. L. Zhu, Sci. Bull. **66**, 2065 (2021)
- 11 M. Ablikim *et al.* (BESIII Collaboration), Phys. Rev. Lett. **129**, 112003 (2022)
- 12 X. K. Dong, F. K. Guo, and B. S. Zou, Phys. Rev. Lett. **126**, 152001 (2021)
- 13 Z. G. Wang, Int. J. Mod. Phys. A **36**, 2150107 (2021)
- 14 R. N. Faustov, V. O. Galkin, and E. M. Savchenko, Universe **7**, 94 (2021)
- 15 X. Y. Chen, Y. Tan, and Y. Chen, Phys. Rev. D **104**, 014017 (2021)
- 16 P. P. Shi, F. Huang, and W. L. Wang, Phys. Rev. D **103** (2021)
- 17 J. Z. Wang, D. Y. Chen, X. Liu, and T. Matsuki, Phys. Lett. B **817**, 136345 (2021)
- 18 M. L. Du, M. Albaladejo, F. K. Guo, and J. Nieves, Phys. Rev. D **105**, 074018 (2022)
- 19 L. Meng, B. Wang, and S. L. Zhu, Phys. Rev. D **102**, 111502 (2020)
- 20 Z. Yang, X. Cao, F. K. Guo, J. Nieves, and M. P. Valderrama, Phys. Rev. D **103**, 074029 (2021)
- 21 Q. N. Wang, W. Chen, and H. X. Chen, Chin. Phys. C **45**, 093102 (2021)
- 22 B. Wang, L. Meng, and S. L. Zhu, Phys. Rev. D **103**, L021501 (2021)
- 23 X. Jin, Y. H. Wu, X. J. Liu, H. X. Huang, J. I. Ping, and B. Zhong, Eur. Phys. J. C **81**, 1108 (2021)
- 24 M. J. Yan, F. Z. Peng, M. Sánchez Sánchez, and M. Pavon Valderrama, Phys. Rev. D **104**, 114025 (2021)
- 25 P. G. Ortega, D. R. Entem, and F. Fernández, Phys. Lett. B **818**, 136382 (2021)
- 26 S. Han and L. Y. Xiao, Phys. Rev. D **105**, 054008 (2022)
- 27 N. Ikeno, R. Molina, and E. Oset, Phys. Rev. D **105**, 014012 (2022)
- 28 X. Cao and Z. Yang, Eur. Phys. J. C **82**, 161 (2022)
- 29 V. Baru, E. Epelbaum, A. Filin, C. Hanhart, and A. Nefediev, Phys. Rev. D **105**, 034014 (2022)
- 30 G. Yang, J. Ping, and J. Segovia, Phys. Rev. D **104**, 094035 (2021)
- 31 Z. M. Ding, H. Y. Jiang, D. Song, and J. He, Eur. Phys. J. C **81**, 732 (2021)
- 32 J. F. Giron, R. F. Lebed, and S. R. Martinez, Phys. Rev. D **104**, 054001 (2021)
- 33 Z. G. Wang, Chin. Phys. C **46**, 123106 (2022)
- 34 M. Ablikim *et al.* (BESIII Collaboration), Chin. Phys. C **46**, 113003 (2022)
- 35 M. Ablikim *et al.* (BESIII Collaboration), Nucl. Instrum. Meth. A **614**, 345 (2010)
- 36 C. H. Yu *et al.*, Proceedings of IPAC2016, Busan, Korea, 2016, doi: 10.18429/JACoW-IPAC2016-TUYA01
- 37 M. Ablikim *et al.* (BESIII Collaboration), Chin. Phys. C **44**, 040001 (2020)

- 38 X. Li *et al.*, Radiat. Detect. Technol. Methods **1**, 13 (2017)
- 39 Y. X. Guo *et al.*, Radiat. Detect. Technol. Methods **1**, 15 (2017)
- 40 P. Cao *et al.*, Nucl. Instrum. Meth. A **953**, 163053 (2020)
- 41 S. Agostinelli *et al.* (GEANT4 Collaboration), Nucl. Instrum. Meth. A **506**, 250 (2003)
- 42 Z. Y. You, Y. T. Liang, and Y. J. Mao, Chin. Phys. C **32**, 572 (2008)
- 43 Y. T. Liang *et al.*, Nucl. Instrum. Meth. A **603**, 325 (2009)
- 44 K. X. Huang *et al.*, Nucl. Sci. Tech. **33**, 142 (2022)
- 45 S. Jadach, B. F. L. Ward, and Z. Was, Phys. Rev. D **63**, 113009 (2001)
- 46 S. Jadach, B. F. L. Ward, and Z. Was, Comput. Phys. Commun. **130**, 260 (2000)
- 47 M. Ablikim *et al.* (BESIII Collaboration), Phys. Rev. D **99**, 052008 (2019)
- 48 P. A. Zyla *et al.* (Particle Data Group), PTEP **2020**, 083C01 (2020)
- 49 M. Ablikim *et al.* (BESIII Collaboration), Phys. Rev. Lett. **112**, 132001 (2014)
- 50 K. S. Cranmer, Comput. Phys. Commun. **136**, 198 (2001)
- 51 R. Aaij *et al.* (LHCb Collaboration), Phys. Rev. D **101**, 032005 (2020)
- 52 M. Ablikim *et al.* (BESIII Collaboration), Phys. Rev. D **104**, 032012 (2021)
- 53 F. Jegerlehner, EPJ Web Conf. **218**, 01003 (2019)
- 54 T. M. Karbach and M. Schlupp, arXiv:1210.7141
- 55 M. Ablikim *et al.* (BESIII Collaboration), Phys. Rev. D **103**, 032006 (2021)